E-beam Lithography using Dry Powder HSQ Resist Having Long Shelf Life and Nanogap Electrode Fabrication

by

Jiashi Shen

A thesis

presented to the University of Waterloo

In fulfillment of the

thesis requirement for the degree of

Master of Applied Science

in

Electrical and Computer Engineering

Waterloo, Ontario, Canada, 2018

AUTHOR'S DECLARATION

I hereby declare that I am the sole author of this thesis. This is a true copy of the thesis, including any required final revisions, as accepted by my examiners.

I understand that my thesis may be made electronically available to the public.

Abstract

As the industry of nanofabrication developing, high-resolution e-beam lithography (EBL) becomes more and more important. In this thesis, it is discussed that the effective factors behind the resolution of EBL and how it works, trying to understand the capabilities and limits of different EBL resists and process to achieve high-resolution patterning. Practically, a new type of EBL resist and its lithography performance are reported. It is a solid state of HSQ. Comparing with traditional DOW-HSQ, it has a longer shelf life and even better contrast. What's more, a resolution boosting method involving two steps of exposure is also reported, which can be applied to fabricate the nanogap in-between block structures (electrodes).

Acknowledgement

Firstly, I would like to express my sincere gratitude to my supervisor Prof. Bo Cui for the continuous support of my Master study and related research, for his extreme patience, kindness and immense knowledge. Without they precious support it would not be possible to conduct this research.

My sincere thanks also go to Dr. Ferhat Aydinoglu, Dr. Ruifeng Yang who help me a lot my my courses and experiment.

Last but not the least, I would like to thank my god: thank you for you let me experience such a lot of things. Relying on you, I overcome all the difficulties and become stronger.

Table of Contents

List of Abbreviation

AFM	Atomic Force Microscope
AQM	Applied Quantum Material
CPU	Central Processing Unit
EBL	Electron-Beam Lithography
EUV	Extreme Ultraviolet
FIB	Focused Ion Beam
HSQ	Hydrogen Silsesquioxane
IC	Integrated Circuit
IPA	Isopropyl Alcohol
MEMS	Micro-Electro-Mechanical Systems
MIBK	Methyl isobutyl ketone
NIL	Nanoimprint lithography
PMMA	Poly (methyl methacrylate)
RIE	Reactive Ion etching
SEM	Scanning Electron Microscope
SERS	Surface-enhanced Raman spectroscopy
TMAH	Tetramethylammonium hydroxide

CHAPTER 1 Introduction

1.1 Overview of nanotechnology:

The integrated circuit with a smaller feature size of elements can be operated faster and with a lower energy cost, which has driven decades of improvement in the semiconductor industry to pursue higher elements density circuit. The famous Moore's law states that the number of transistors working on dense integrated circuits will double every two years[1]. As the ultimate size of the transistor has achieved a nanometer scale, keeping this advancement becomes harder and the involving fabrication technology is named nanotechnology[2].

Nanotechnology is defined as the manipulation of matter with at least one dimension in nanoscale, that is 1 to 100 nm[3], where the error range of size and feature boundary derived from traditional fabrication will become huge and effective to the performance of a certain functional structure or say nanoelements. Therefore, achieving the ultimate possible resolution pattern has become the crucial task of nanotechnology applied in semiconductor fabrication.

1.2 Process of nanofabrication

A regular processing flow of nanofabrication includes three main components: deposition, lithography, and etching as shown in Figure 1.2. Other techniques such as

doping (ion implantation) are also important for a semiconductor device. But the building of structure is mainly completed by operating an orderly combination of these three steps.

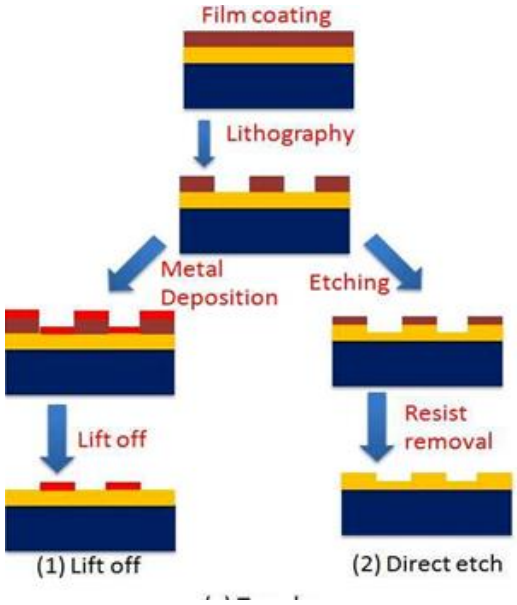

Figure 1.1. A general processing flow of nanofabrication

Generally, the process starts with bulk material. Through deposition[4], a layer of material, such as metal, a semiconductor and dielectric or resist film will be added on the substrate. Thickness can be controlled with different accuracy depending on respective deposition technology.

Then the shape in other two dimensions can be defined by patterning step. Most patterning technology can be summarized as exposing electromagnetic wave or particle beam flow over related lithography resist. Such a film should be sensitive to corresponding exposure, and its solubility will be significantly changed after being exposed. In most situations, since this radiation has a short wavelength, and is controllable by an electrical

signal, the designed figure can be transformed on resist film with small size and high resolution. Resist will basically play two roles. Following with deposition, they can define deposited material with the designed pattern by lift-off[5] as shown the left steam of Figure 1.1. Or they can protect material under a certain area from etching, as shown in the right steam. [6]

Figure 1.2 Image of an integrated circuit with different layers, form Lucent Technologies.

Etching, as the name suggests, will remove substrate materials from the processed sample. Frequently used etching method can be classified as reactive ion etching (RIE), ion beam etching, wet chemical etching, polishing and so on. The lithography resist material processed on the last step is expected to have good etching resistivity, so that, the pattern defined on film will transform to the layer under it. The top view of a complete electrical element may have different patterns from top to bottom, as shown in Figure 1.2.

To fabricate an integrated circuit with millions of such elements, it is necessary to repeat the previous processing for each layer.

From the above description, it is obvious that the quality and accuracy of all steps during fabrication will affect the final resolution. Similar to all the other processing flow, the worst step can limit the final resolution of the whole system. For some special projects dealing with a very thick layer of materials, the etching step may become the limiting factor. But in most situations, the most critical step is patterning. The following part of this chapter will discuss the patterning method more specifically.

1.3 Patterning method

Patterning method in modern nanotechnology mainly relies on lithography technology such as photolithography, electron beam lithography, X-ray lithography[7], nanoimprint[8] (NIL), and so on.

1.3.1 Photolithography

In photolithography, light with a certain wavelength is exposed over a layer of light-sensitive chemical film through a well-prepared photomask with the designed pattern. On the resist layer, the area shadowed by the opaque part of the mask is protected from exposure while other area will be exposed where some light-driving chemical reaction occurs. Then the geometric pattern on a photomask will be transferred to the photoresist.[9]

Photolithography is commonly called optical lithography and UV lithography. There are three exposure methods of optical lithography: contact printing, proximity printing and projection printing. For contact printing, as the name implies, the mask is placed in contact with the photoresist, so that pattern transformation is accurate and reliable. However, this method will introduce a lot of contamination to the system and the cost from mask wear is also considerable. The best resolution that this method can achieve is about 0.5 μm. Since the mask can be used for about 20 times only, it is abandoned by the IC industry in the 1970s.

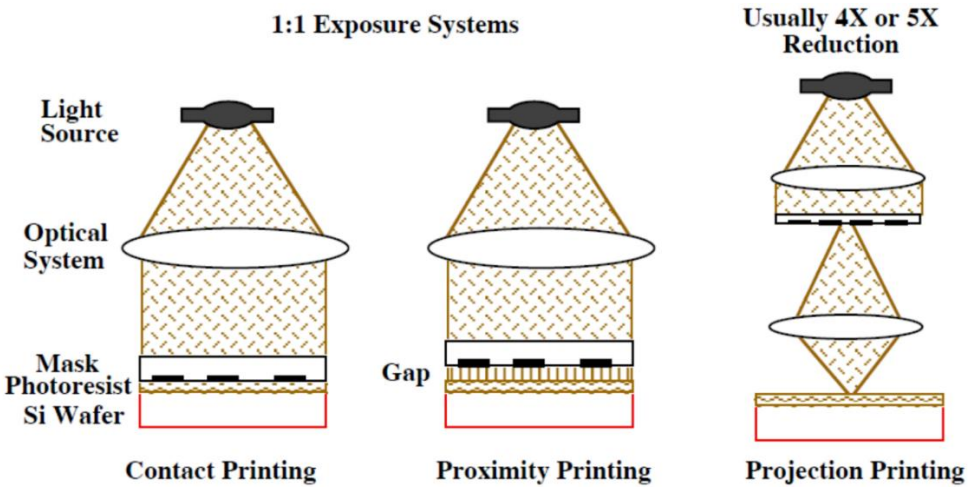

Figure 1.3 Three different types of optical lithography

A compromising solution is to put the mask over the photoresist as close as possible but without contacting it, which is named proximity printing. In this case, contamination and erosion will greatly decrease in the cost of resolution depending on the distance between the mask and resist. The third method is projection printing[10], where the mask

is placed above the resist film at a suitable distance. Light exiting from the mask will be focused by an optical lens in between the mask and film to form an image of the pattern on the film. This method has no contamination, but the cost of the whole system is the highest. What's more, after several upgrading, the most advanced projection printing can achieve 10 nm resolution [11].

The working principle of optical lithography determines that the final size of pattern achieved on the resist is comparable with the pattern on the mask. This scale is 1 over 1 for contact and proximity printing. The best demagnification is acquired by projection printing, which is generally 4 or 5 times. That means if optical lithography is going to be used in nanotechnology, it is necessary to fabricate a mask in nanoscale first. In other words, the technique of optical lithography is not able to bridge the gap between macroscale and nanoscale.

While the semiconductor industry has been using SEBL-generated photomasks for optical projection lithography in much the same way for decades, resolution of this method is theoretically limited by the wavelength of light. Other factors such as the thickness of the mask and index of refraction of all optical elements in this system will decrease this resolution further. In industry, rare UV optical lithography equipment can achieve sub-micrometer accuracy. Therefore, this technology is used to fabricate some low-price chip, which does not require high performance.

To extend the resolution, Deep UV or extreme UV lithography is developed where the wavelength of exposure is reduced. In short, characteristics derived from using mask are similar to photolithography, but shorter wavelength gives them higher resolution[12], which can achieve sub 10 nm in manufactory industry. One significant difference of EUV lithography from optical lithography is that the material absorption of the short wavelength wave is high[13], which will affect the design of mask material. Radiation and contamination risk of this method is considerable.

In short, given that the photolithography uses a mask to define the pattern, on which every point is exposed at the same time, people can improve the productivity dozens of times by arranging repeating patterns on a larger wafer. What's more, the present EUV lithography technology has already pushed the resolution to sub-10 nm[14], so it is generally used in the most advanced CPU fabrication nowadays.

1.3.2 Electron beam lithography

Electron beam lithography is a kind of direct-write lithography rooted in Scanning Electrical Microscopy (SEM)[15]. Its working principle is described in the following paragraph. Plenty of electrons are accelerated through the high voltage electrical field to form an electron beam[16]. This divergent beam, emitted from the gun, will converge to a focused spot on the surface of the sample through an electromagnetic deflection system which plays the role of the optical lens. During the lithography procedure, the focused

electron beam scans over the wafer coated with e-beam resist whose solubility will change after being exposed.

As the SEM was steadily improving in recent decades, higher quality equipment with more accurate pattern generators and higher energy acceleration systems improved the resolution of EBL to sub-10 nm level[17]. Compared with photolithography, EBL skips the steps of mask preparation. Therefore, it has good flexibility in pattern change. However, this character also has a negative side. Since the pattern is defined by focused e-beam spot, every single pixel has to be exposed one by one, thus the processing time and cost is proportional to the area of the pattern. Although its throughput is low, it is still appropriate to some applications where resolution is concerned, but throughput is less critical.

1.4 Thesis contribution

In this work, we seek to understand the capabilities and limits of different EBL resists and process to achieve high-resolution patterning. As we have seen, exploring higher resolution EBL techniques is meaningful and constructive to the development of nanotechnology. Quite a bit of work around high-resolution lithography has been done in recent years, aiming to improve the resolution through all kinds of method. Therefore, the first part of this thesis will discuss the effective factors behind the resolution of EBL and how it works.

The experiment part will report two projects. The first one is about testing a new type of HSQ resist in the powder form. To evaluate the performance of a lithography resist,

some basic properties such as spin coating parameter, sensitivity, and contrast are tested. This new type of resist is used to define a dense line array to explore its ultimate resolution potential.

The second project is using two-step exposure EBL to fabricate nanogap. To explore the ultra-narrow gap, some resolution promoting methods, which were proven effective by previous works, are applied. Different from some other study regarding high-resolution EBL, this project is dealing with block structures with nanogap in-between rather than isolated nanostructure.

CHAPTER 2 Introduction to EBL

2.1 Structure of Electron Beam Lithography system:

The ultimate purpose of EBL is to produce high-resolution and high-density patterns, which depends on a series of factors including beam size, the choice of resist and developer, and also the process parameter of development. From the point of EBL equipment, the key is to generate a well-focused beam spot [18].

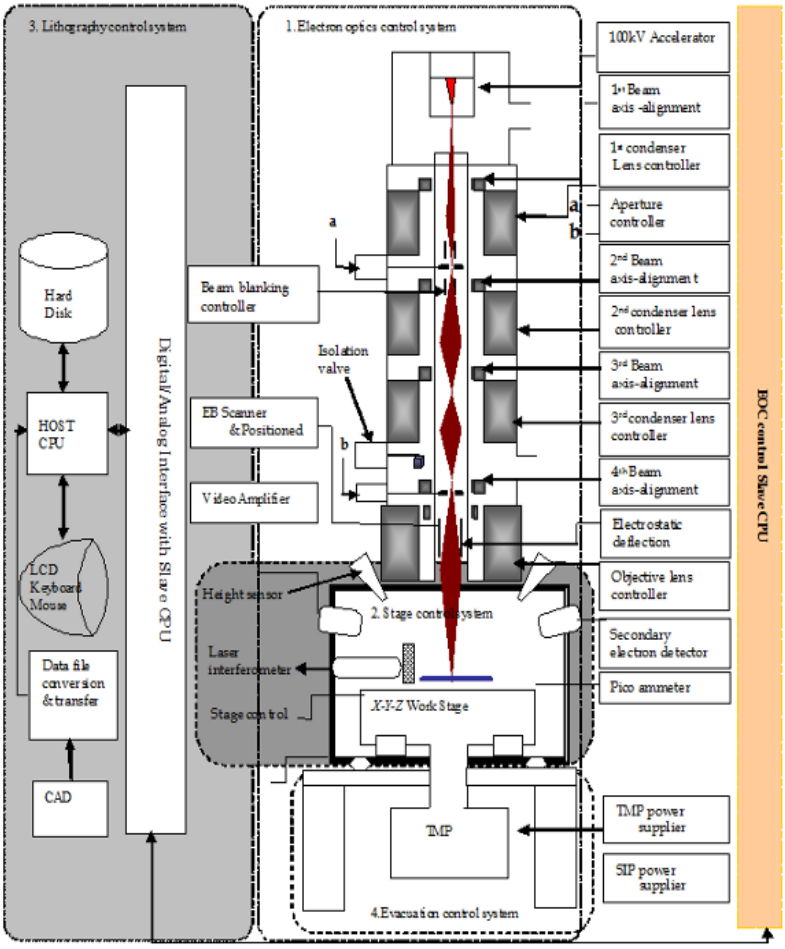

Figure 2.1 Schematic drawing showing the major components of a high-energy electron beam lithography system. [Cen Shawn Wu, 2010]

2.1.1 High-power E-beam generator

Electron flow is generated by an electron emission gun and is accelerated to achieve high energy through the following accelerating electrical field.

The electron emission gun can be divided into three categories [18]:

1. Thermionic emission gun.
2. (Cold) field emission gun
3. Schottky emission gun

The thermionic emission gun is working at a high temperature; some electrons constrained in the materials of the tip can acquire enough thermal kinetic energy (larger than its negative potential energy) to jump into the vacuum. These electrons are then attracted and enter the accelerating electrical field following the emission gun. The material of the thermal tip is generally chosen as W or LaB6.[19] Compared with the other two types of gun, it is cheap to make and use, and only a modest vacuum is required. However, it is not a sharp beam source.

The cold field emission gun is operated at high field and high voltage (several kilovolts) which provides enough potential difference to emit the free electrons inside the metal to outer vacuum space. The generation of E-beam is independent of temperature. Therefore, this type of gun is held at room temperature and is thus called cold field emission gun. This kind of gun has a sharp tip with a diameter of about 100 nm, so the emitted beam has better convergence. However, it still suffers from serious contamination since the gas

molecules from the approximate vacuum environment are easier to be absorbed and built up contamination at low temperature. This electron gun needs an ultra-high vacuum and is not ideal.

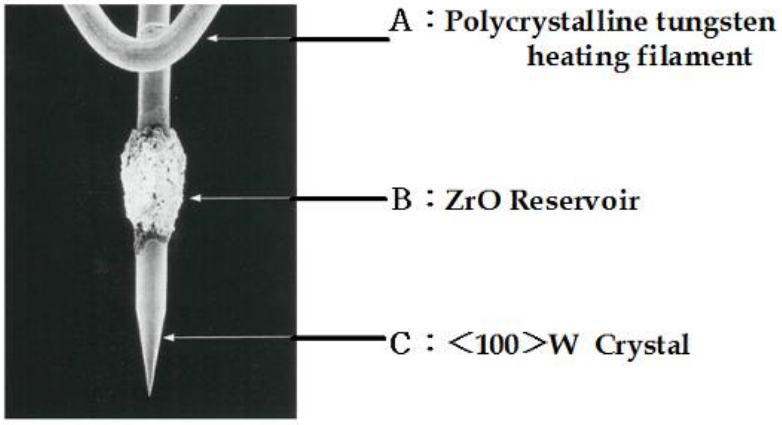

Figure 2.2 One type of common applied Schottky gun: ZrO/W thermal field emission electron source. [Cen Shawn Wu, 2010]

The Schottky gun, also called a thermal field emission electron source[20], is operated at a high temperature as well. Shown in figure 2.2. The high electric field is also applied on the tip of the Schottky gun which can help electrons standing on a high potential state. The cathode of it is fabricated by tungsten with about a 1 μm diameter. This type of gun combines the advantages of the former two emission guns: 1, the convergence of beam flow from it is much better than the thermionic guns; 2, it is compatible with a lower vacuum environment; 3, it requires a relatively low electrical field; 4, it has low wear and contamination level, and therefore, has a long life and is economical. In short, this type of electron emission gun is matured and is generally used in the EBL system.

2.1.2 Accelerator

Following the gun, an accelerator will further speed up electrons to energy level from several keV up to 100 KeV[21]. The different kinetic energy that the beam currents have is not very critical to the beam size. But it will affect the energy deposition of the E-beam on the resist material and further affect the resolution. It is more about proximity effect, which we will discuss it in Part II. Generally, it is recognized that the higher the acceleration voltage the beam has, the higher the resolution that can be achieved.

2.1.3 Electron-optical system

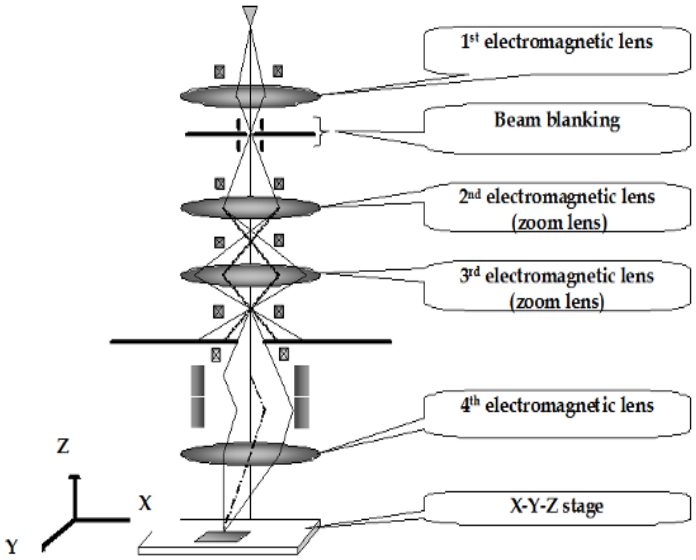

Figure 2.3 Schematic drawing showing the structure of electro-optic components on an EBL system[Cen Shawn Wu, 2010]

Then the accelerated electron beam will be focused to a spot with a size of about 2 nm by a group of electromagnetic lenses. There are four electromagnetic lenses working

together here: one is working as the focusing lens and other three for zoom lenses so that the reduction ratio of the beam diameter and the irradiating current are adjustable.

Before the beam enters each lens, it is necessary to be aligned with the center of the optical axis of the electromagnetic lens. This function is completed by the beam axis alignment coil[18][22], which essentially is an electrified coil which can produce a magnetic field, so the deflection of the electron beam can be accurately controlled by an electrical signal.[23]

2.1.4 Astigmatism corrector

As a deviation from ideal case, the beam can focus on an elliptical area rather than a point or a circle, which is called astigmatism and is caused by an electron beam being forced unevenly in different directions all over the electromagnetic field. Generally, two reasons will bring such asymmetry of electromagnetic force in different directions: 1) flaws in the equipment, and 2) contamination.

If there is astigmatism, the image of the object will be stretched in different directions while the focus is being adjusted, as shown in Figure 2.4. Even though the image is isotropic when it is well focused, the sharpness and resolution of the image are still very weak, since the beam spot size is larger than ideal case. Therefore, the final resolution of lithography will be decreased. [18]

Similar to beam axis alignment, astigmatism correction is completed via an astigmatism corrector, which consists of several electrified coils in different angles to each

other. While operating the SEM equipment, this corrector can be controlled artificially depending on the operator's judgment. Obviously, there is no guarantee that this correction is completed with high accuracy and reliability. Therefore, at high-resolution lithography with a scale under 20 nm, the operation of equipment and whether astigmatism can be well corrected will become a limiting factor of the achieved resolution.

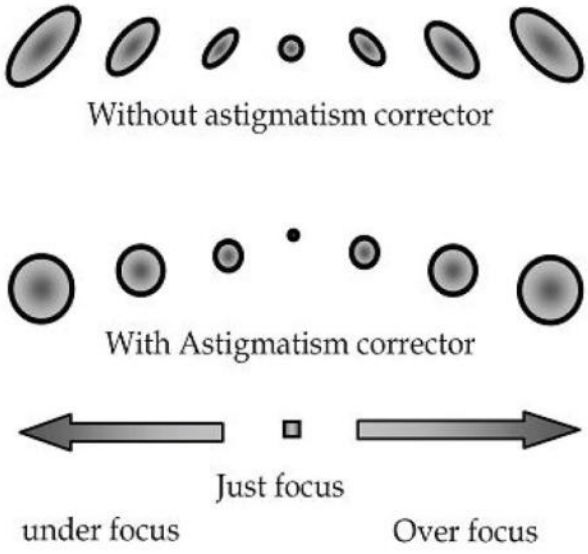

Figure 2.4 Schematic drawing showing the structure of electro-optic components on an EBL system [Cen Shawn Wu, 2010]

PART II.
E-beam Lithography using Dry Powder HSQ Resist Having Long Shelf Life

CHAPTER 3 Basic Property of AQM-HSQ Resist

3.1 Background and motivation

As mentioned before, the development of high-resolution EBL lithography is very important to modern nanotechnology, which has broad applications ranging from high-density magnetic storage[24], integrated circuits, nano-sensor and nano-photonic devices[25]. Among all types of e-beam sensitive materials, PMMA is one of the most popular EBL resists because of its high-resolution, low cost, long shelf left life and reliability[26]. But it is of a positive tone, which is not always applicable to every application because the ratio of the exposed area over the unexposed area should be designed as small as possible, or the final resolution will be degraded due to proximity effect. Furthermore, a large area patterning will significantly increase the exposure time; therefore, for such purposes, a negative resist is necessary.

Unfortunately, no negative resist exists with similar properties to PMMA, and some of the commonly used negative e-beam resists are SU-8, calixarene, polystyrene, and HSQ [27]. SU-8 is a chemically amplified resist, has very high sensitivity but low contrast[28]. Calixarene has high-resolution, but it is low in sensitivity[29]. Besides that, it will generate acid during exposure that will corrode nearby structures or materials on the sample. Polystyrene, which has a good compromise between contrast and sensitivity, can achieve resolution of ~10 nm[30].

Hydrogen silsesquioxane (HSQ) is a popular inorganic resist in a negative tone. It plays an important role in the research of nanofabrication because it has good etching resistivity [31], low linewidth roughness[32] and very high-resolution capability. It is reported that isolated 7 nm wide lines can be achieved when using 100 KeV e-beam and 20 nm thick resist[33]. And Joel K. W. Yang et al. reported that 9 nm pitch was obtained at 10 KeV acceleration voltage combined with salty development[34]. However, there is one notable drawback of using traditional HSQ resist. The shelf life of this liquid resist is too short that limits its wide usage. According to the sales specifications of Dow Corning® XR-1541 E-Beam Resist, these products should be stored at 5 ºC and will expire within six months from the date of manufacture. Compared to another popular positive tone resist PMMA, which is considered to have no shelf life issue at room temperature and in a standard humidity environment, the storage time and temperature requirement of HSQ make it costly to purchase, transport and use. Consequently, researchers are looking for a more advanced negative resist.

In this section, a form of Hydrogen silicon oxide polymer resin will be introduced, which has the same chemical formula, $[HSiO_{3/2}]_n$, as traditional HSQ but is a dry powder that can be stored for a long time[35]. It will be referred as AQM-HSQ (AQM: Applied Quantum Materials Inc., the Canadian company making the HSQ resist), and traditional HSQ will be referred to as Dow HSQ in the following. This product can be stored in a room environment. For preparation before usage, it can be dissolved in methyl isobutyl ketone (MIBK) or toluene. However, this resist still does not solve another problem with HSQ.

That is, the coated HSQ film is not stable for the humidity in the air and must be exposed and developed quickly to attain the reproducible result [36]. Here, we study the contrast and resolution properties of AQM-HSQ.

3.2 Resist coating

Spin coating of resist material on a bare semiconductor wafer as a thin layer is generally the first step of fabrication involving lithography. The thickness of the film will affect the performance of resist on the following step. For example, the thicker resist is more likely to collapse if the developed pattern is very small from the top view. But higher resist structure may be more enduring during dry etching. For a project that needs high resolution, a thinner resist may be more appropriate.

For each specific experiment, the researcher needs to decide the thickness of the film to be used based on different purposes. In this report, a 200 nm thick film is used to measure the contrast curve and thin film no more than 30 nm is applied for the exploration of ultimate high resolution.

For a spin coating to deposit resist film on the wafer, there are two factors, which may affect the thickness of the film: 1) rotating speed; 2) concentration of resist solution.

Given the centrifugal force, the thickness of the film will decrease as the spin speed increases. Most of the reported experiments use the spin speed ranging from 1000 rpm to 5000rpm. Too low speed may not spread the resist solution all over the wafer evenly. On the other hand, the spin speed higher than 5000rpm cannot significantly reduce the

thickness further. Under this circumstance, the researcher can dilute the resist solution to decrease its viscosity, and thinner resist can be achieved. Moreover, the effect of both of these two parameters on the film thickness is not linear.

Considering different properties of the various materials, it is necessary to measure the spin coating curve of AQM-HSQ powder. That is the first step of this project and will also provide a reference to the subsequent user.

3.3 Contrast curve

3.3.1 Fundamentals of resist contrast

Resist contrast is an important property to determine the performance of a resist. Since there is an inevitable problem of proximity effect, electrons cannot always be deposited on the position as it is designed. This spread of energy can cause a decrease in resolution. However, the energy absorbed by the area close to the designed feature is generally lower than that on the aimed area; and if it is also lower than the required threshold dose of the applied resist, it may not cause unexpected pattern enlargement.

Though we can control the dose of proximity exposure to be under threshold by decreasing the total dose injected on the designed area, this may also degrade the quality of the pattern that is wanted. Therefore, it is desired that there is a clear boundary between the non-response dose range and 100% effective dose range.[37]

However, such an ideal resist does not exist in the real world. One still wants the transition region to be as narrow as possible. This discriminability of resist to reply on different exposure dose is defined as contrast. Traditional HSQ is typically developed in

an aqueous alkali solution such as TMAH (tetramethyl ammonium hydroxide), which results in a low contrast. To improve the contrast, several development techniques have been studied, such as high concentrate development[38], thermal development[39][40], KOH development[41] and salty development[42]. The hot or concentrated developers are not suitable for some substrates/films such as silicon because they can etch silicon. A salty developer would be a meaningful choice. Here, we hypothesize the AQM-HSQ has similar function group to traditional HSQ[43], so that TMAH and high-resolution salty developer are used in this experiment.

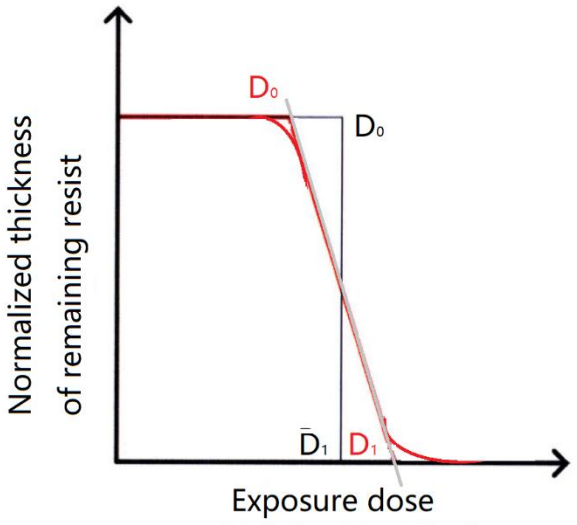

Figure 3.1 Contrast curve plotting for ideal resist (black) and realistic resist (red)

Contrast calculation of resist is generally obtained by exposing an array of squares with the size of several microns on a thick resist film at an exponentially increasing dose. After development, one measures the height of the remaining resist and plots them (normalized to initial thickness, therefore less than 1) with the corresponding dose. Figure 3.1 shows an example of the contrast curve for a positive resist. The ideal resists (black line) as described before have a vertical part on the contrast curve.

The real resist (red) has a transition curve region with finite slop between zero response (denoted as D_0) and saturated dose region (starting from D_1). In practice, since the transition region is not a straight line, a trend line of these data points will be added, and the intersection point of this trend line with zero and 100% height level will be chosen as D_0 and D_1.

As labeled on the above figure, the contrast value is determined by the formula:

$$\gamma = \left[\log\left(\frac{D_1}{D_0} \right) \right]^{-1}$$

where the " γ " denotes contrast. Higher γ value implies better contrast and corresponds to a steep slope of the transition curve.

Contrast property is primarily dependent on the property of resist and may also be affected by other parameters, such as the thickness of resist layer, different developer, develop time and temperature. Therefore, contrast is not an intrinsic character of resist. However, this provides the researcher with abundant methods to enhance contrast in the practical experiment, which will be discussed in more detail in the next chapter.

3.3.2 Experiment procedure

To utilize this AQM-HSQ powder, the resist solution is firstly prepared. Solid AQM is dissolved into MIBK as 6 wt./vol % solution. In the following steps, this basic solution will be diluted to different concentration.

Then, the bare silicon wafers used as substrates are cleaned by Reactive Ion Etching (RIE) in O_2 plasma cleaning recipe for 5 mins, followed with ultrasonic cleaning in acetone and then rinsed by isopropanol alcohol (IPA). Since the AQM-HSQ is as sensitive to

moisture as DOW HSQ, the cleaned wafers are dehydrated at 180℃ for 20 min. Then the samples are spin coated at 3000rpm for 60s. Following the spin coating, soft bake the sample for 90℃, 4min on a hot plate. After spin coating, the thickness of the sample is checked by using Dektak profilometer, and the measured thickness is 210 nm. To make a comparison, the sample of conventional Dow-Corning HSQ were also prepared and the thickness is 215 nm.

The e-beam exposure is done by Raith 150 system. Since the requirement of resolution is not very high to measure contrast curve, the lithography is operated with 10 mm working distance and 30 μm aperture size, the step size is 50 nm, and the acceleration voltage is 20 KeV. After lithography, samples are developed by 25 % TMAH (tetra methyl ammonium hydroxide) for 70 seconds, or with the high-contrast salty developer[44], that is 1 wt% NaOH and 4 wt% NaCl for 2 min, followed by DI water rinse. One important point is that, if the salty development is applied, the rinse time should be not less than 2 min, and the longer, the better. Otherwise, the remained salt will crystallize on top of the substrate. In this project, 5 min is applied.

For traditional TMAH development, a dose array from 80 μC/cm^2 to 1500 μC/cm^2 is used and dose multiplication factor is 1.0476 exponentially. And, for salty development, higher exposure dose is necessary. After taking several attempts, it is determined that the dose range from 200 μC/cm^2 to 4109 μC/cm^2 is utilized.

3.4 Result and analysis

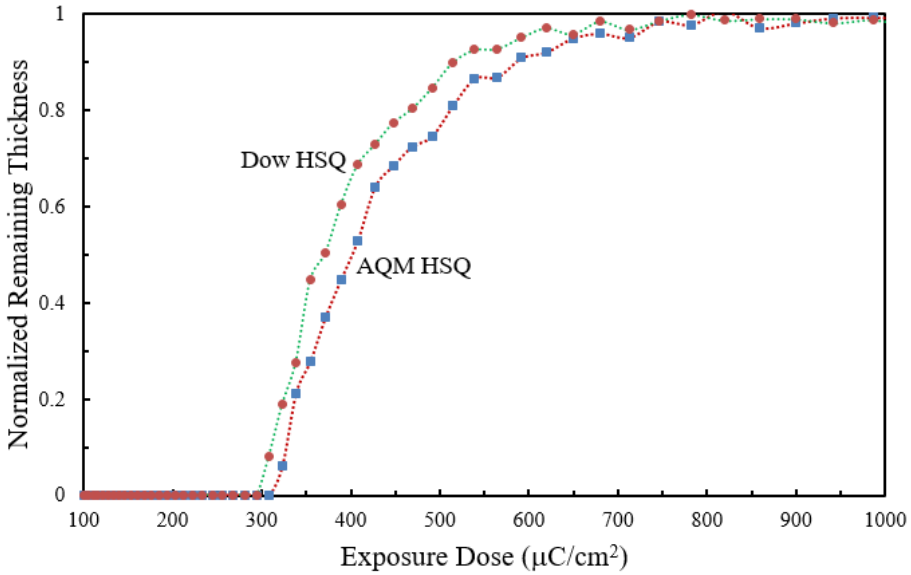

Figure 3.2 Contrast curve of AQM HSQ and Dow HSQ using TMAH

Figure 3.2 shows the plotted chart of the contrast curve of AQM-HSQ and Dow HSQ resist using TMAH to develop. The vertical axis represents the remaining thickness of the resist after development, and the dose of exposure is the independent variable. The value of resist height is normalized by the original thickness, which is 215 nm for AQM HSQ and 210 nm Dow HSQ respectively.

	AQM HSQ	Dow HSQ
Thickness (nm)	214	208
Contrast	4.83	5.01
Sensitivity D_{50} (μC/cm2)	407	354

Form 3.1 Contrast data using TMAH development

Figure 3.3 shows the contrast curve of the both resists with high-resolution salty development.

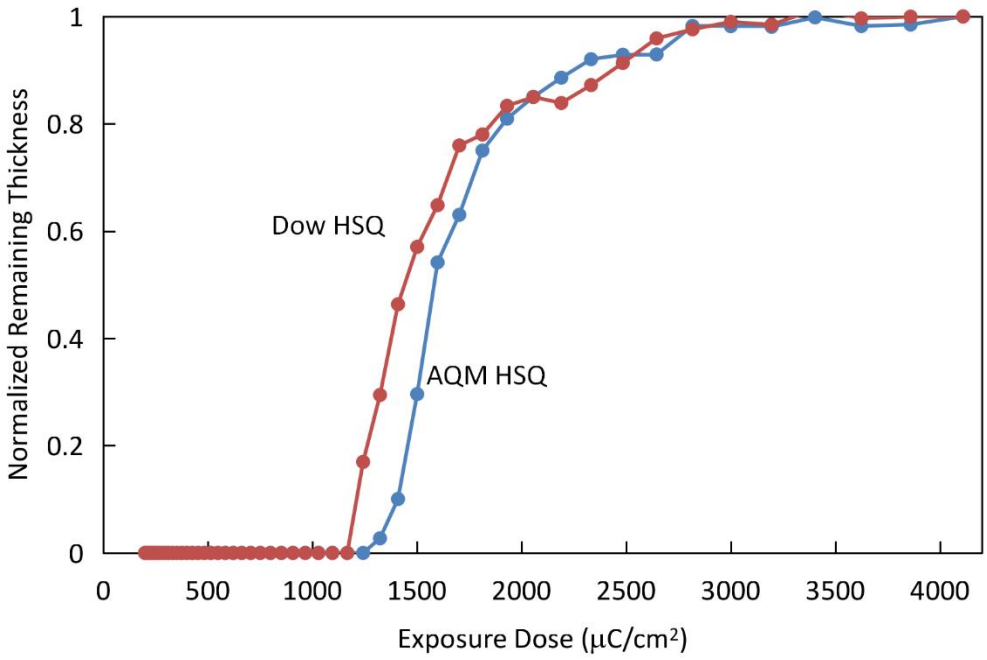

Figure 3.3 Contrast curve of AQM HSQ and Dow HSQ using salty development

The threshold dose for AQM-HSQ and Dow HSQ are 1320 μC/cm^2 and 1240 μC/cm^2, and the saturation doses are 2820 μC/cm^2 and 3000 μC/cm^2, respectively. As a result, this new powder form of HSQ has a more advanced contrast, although the sensitivity is slightly lower. These two properties are quantitively summarized in Table 2.

	AQM HSQ	Dow HSQ
Thickness (nm)	260	261
Contrast	8.66	7.01
Sensitivity D_{50} (μC/cm2)	1600	1450

Form 3.2 Contrast data using salty development

This result shows that, compared with the TMAH method, the salty development method can enhance the contrast of HSQ resist. Furthermore, this enhancement is verified to be effective to AQM-HSQ resist as well. Although the exact development mechanism has not been well understood, we can still infer that AQM-HSQ resist has the same or chemically similar reaction during development.

Secondly, the AQM HSQ resist has a higher contrast but lower sensitivity than Dow HSQ. This difference is less obvious for TMAH development. And given the inaccurate measurement of thickness and the choice of points, AQM-HSQ seems to have a little lower value of contrast. However, in the experiment of high-resolution salty development, AQM-HSQ performs a very high contrast, which gives AQM HSQ a high-resolution potential. The contrast is high enough, so that it is no longer the limiting factor of resolution in sub 10 nm fabrication processing. It can be seen that this new resist is competitive to existing HSQ and positive PMMA.

Thirdly, like all other EBL or photoresist, higher contrast is always accompanied by a lower sensitivity.

CHAPTER 4 High-Resolution EBL Using AQM HSQ Resist

4.1 Experiment Procedure

In this experiment, to obtain high-resolution patterns, 1% solution of AQM-HSQ was spin coated on a bare silicon wafer at 5000 rpm. This film is evenly 30 nm thick checked by Dektak. To avoid the thermally induced contrast degradation, soft bake was not carried out [45]. Lithography was performed 20 mins after spin coating.

To test the performance of AQM HSQ in ultra-high resolution writing, three different pattern types: 1) nested ”L” structure, 2) dot array and 3) bowtie structures were tested.

1) Nested – “L” structures

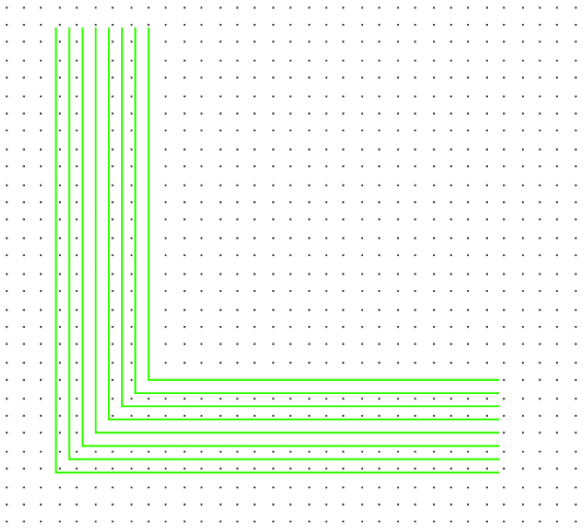

Figure 4.1 Layout of line test pattern

As shown in the figure 4.1.1, a pattern of single pixel “L” sharp line with no width are applied.

The period of line patterns ranges from 10 nm to 35 nm in step of 5 nm. The original dose is 1.5 nC/cm, and the multiplication factor is 1.065.

2) Dense dots array

Single pixel dot arrays[46] in 10 by 10, with periods ranging from 15 nm to 25 nm, were exposed at 0.0006 pC.

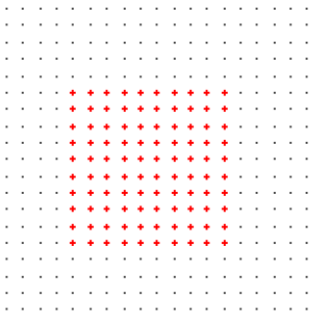

Figure 4.2 Layout of dots pattern

3) Bowtie structure

Bowtie structure shown in figure 4.3 with a lot of applications, such as nano-antenna[47] is also tested in this project. It uses area dose from 1500 μC/cm^2 with a multiplication factor of 1.065. The gap sizes between the two triangles range from 2 nm to 16 nm.

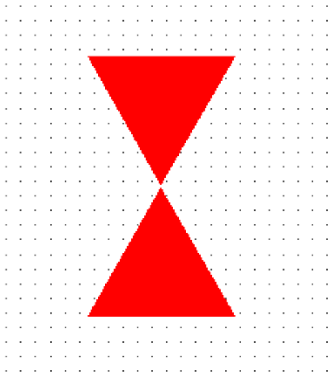

Figure 4.3 Layout of the bowtie pattern

The e-beam exposure was carried out at 25 keV followed by the high-contrast salty development for 15 secs followed by DI water bath for 5 min.

The ultimate resolution of EBL depends on not only the resist performance[48], but also how tightly the beam spot focus[49] and the proximity effect occurring on the sample. Therefore, in this part of the experiment, 25 KeV is used, which is the highest allowed acceleration voltage by QNF, and the lithography is operated with 8 mm working distance and 10 μm aperture size, and the step size is 6 nm.

After lithography, all the samples are developed by the high-contrast salty developer, which is verified to yield high contrast for HSQ in the last chapter. Development time is 15 secs followed by DI water rinse for 5 min to completely remove the salt.

To avoid the aging effects[50], all steps from the spin coating to development have been completed within 12 hours.

4.2 Result and analysis:

4.2.1 Line pattern result

The figure 4. 4 shows the result of nested “L” structure with 7.5 nm half-pitch and 10 nm half-pitch. Fig 4.4 a) is 15 nm pitch line pattern and b) is 20 nm pitch line pattern.

The patterns are well defined while the resist is quite thick compared to the pattern density. Figure 4.5 shows the AFM measurement of the height of the pattern as 34 nm. The world record of dense line pitch is 9 nm, however, it is achieved by using thinner film of 10 nm. For thick resist film, the best-reported result is a 15 nm pitch with 7 nm line width.

This result verifies that this new type of AQM-HSQ powder has as good performance as traditional HSQ solution

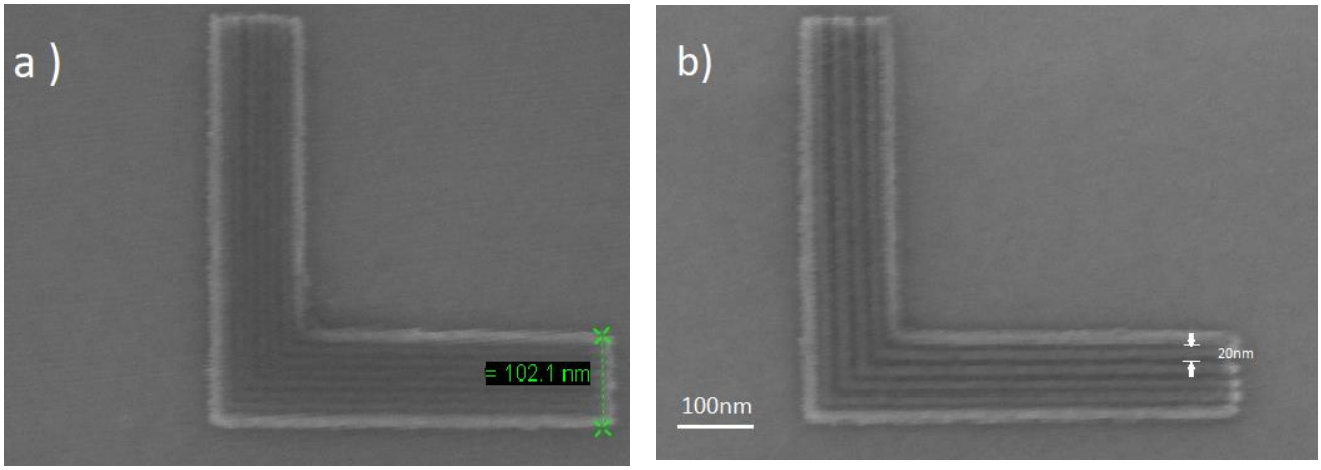

Figure 4.4 SEM image of nested “L” structure structures fabricated at 25 KeV using 35 nm thick film. a) 7.5 nm half-pitch, b) 10 nm half-pitch.

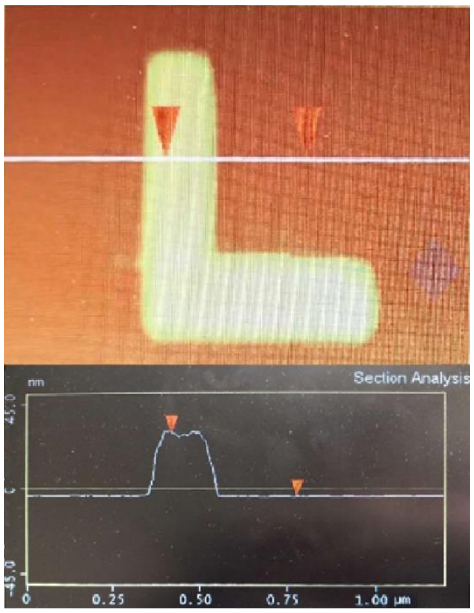

Figure 4.5 Thickness profile of line pattern measured by AFM

Figure 4.6 shows the result using TMAH developer. The best resolution that can be acquired by this method is 50 nm pitch, which is significantly worse than using the salty

development method. This result verifies that the new type AQM-HSQ powder has a similar reactive mechanism.

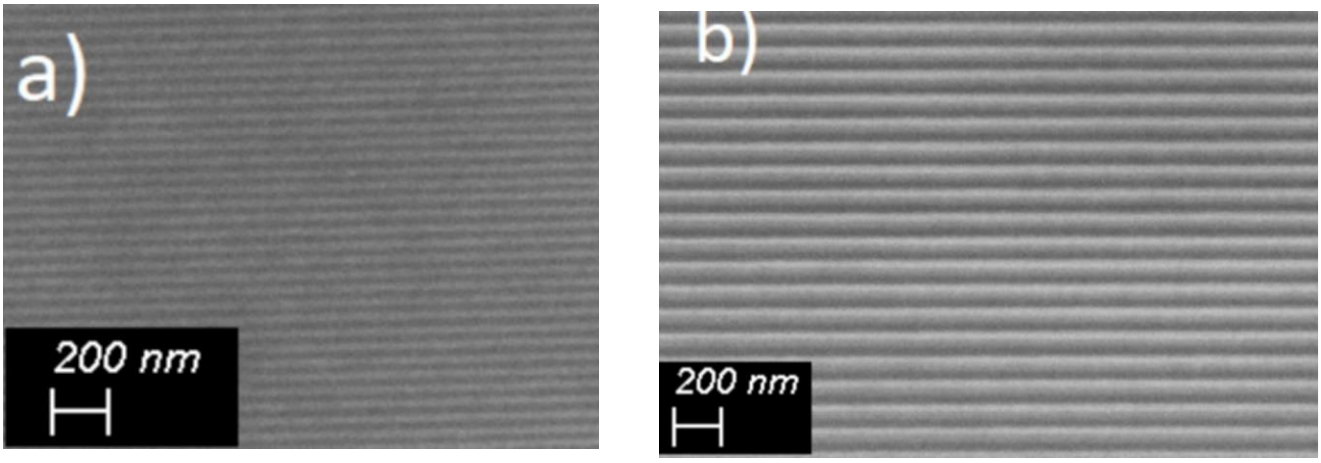

Figure 4.6 SEM image of TMAH method exposed by Raith 150 system at 25 KeV. a) 50 nm pitch and b) 100 nm pitch

4.2.2 Dots pattern result

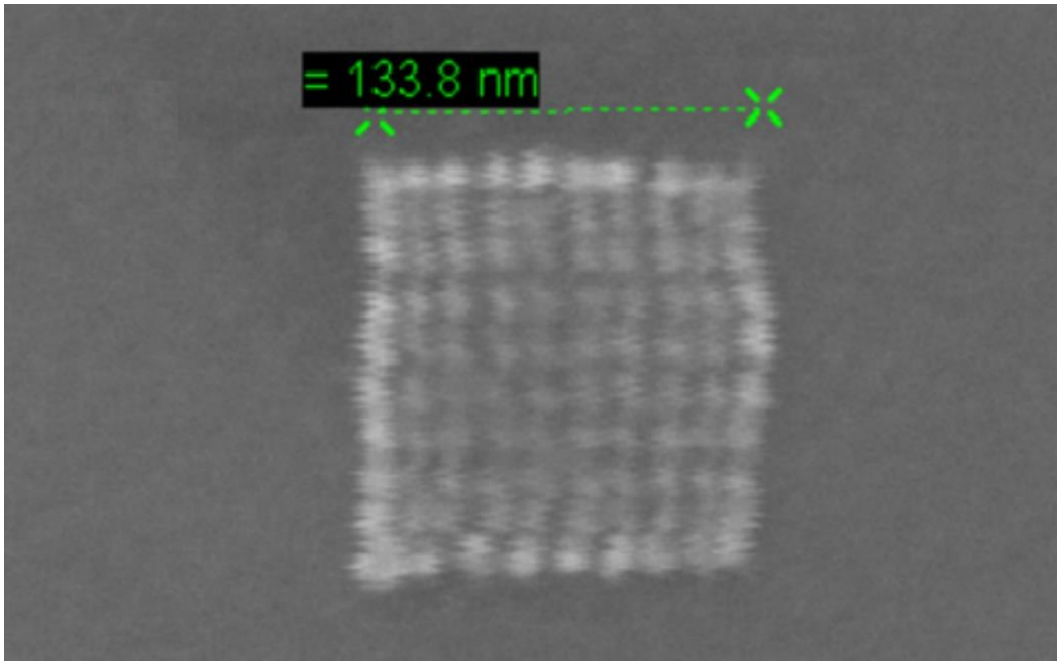

Figure 4.7 SEM image of 7.5 nm half-pitch dense dot array using 40 nm thick film exposed by Raith 150 system at 25 KeV

As shown in figure 4.7, the best result achieved for dense pillar array is 15 nm period. The thickness of this resist is 40 nm. Therefore, its aspect ratio is about 5.

4.2.3 Bowtie pattern result

As shown in figure 4.8, the best result of bowtie structure can approach ~5 nm measured gap, while it was originally designed with a 2 nm gap. This result demonstrates that AQM HSQ, in a negative tone resist, is good enough to be utilized in the fabrication of nano-antenna.

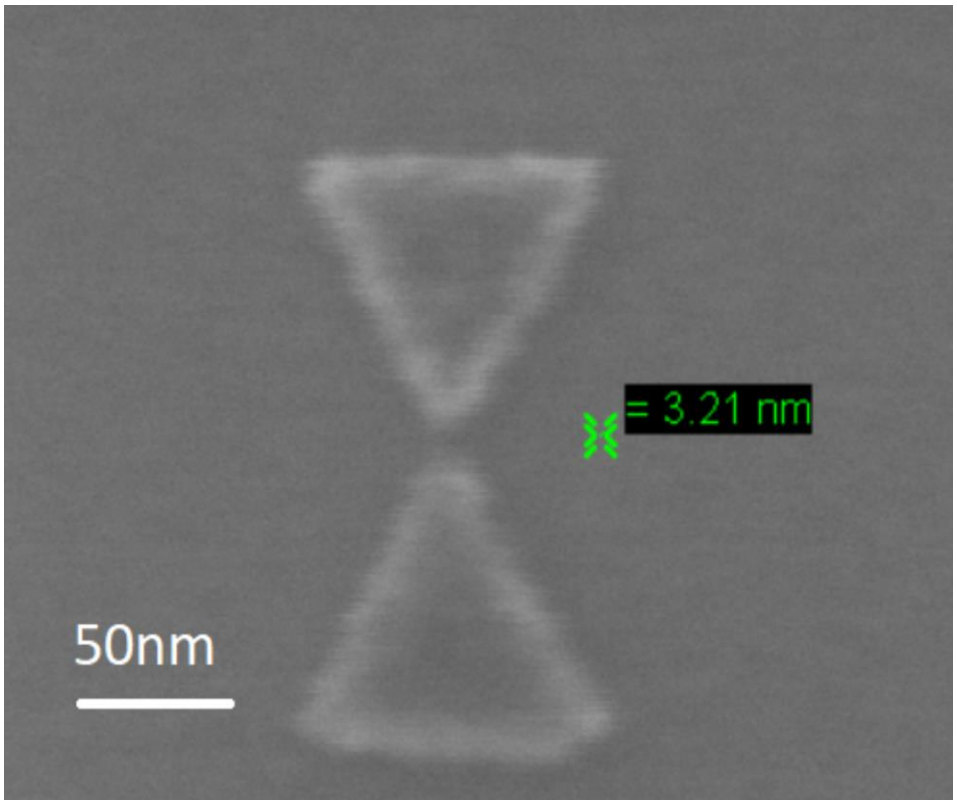

Figure 4.8 Image result of the bowtie structure pattern

4.3 CONCLUSION

It is demonstrated that the AQM-HSQ as a powder type HSQ resist is stable, can achieve 7.5-nm-half-pitch structure by using high-resolution salty development process. Compared with traditional HSQ, using salty developer or other contrast improving method in similar equipment and at equivalent acceleration voltage, AQM-HSQ can produce the same or even better performance. Moreover, it presents promising mechanical strength at high aspect ratio patterning. The result of this article implies that this new type of material could be used as an alternative negative e-beam resist with long shelf life, low cost and high resolution. However, before applying AQM-HSQ widely, there are still some issues to be studied, such as patterning transfer to the bulk material, etching selectivity over other substance, and so on.

PART III.
Nano-Gap Fabrication

CHAPTER 5 Fabrication of nanogap structure

5.1 Background of nanogap

The concept of nanogap can be defined as the narrow gap between two patterns with nanoscale feature size. Without a doubt, it is a fundamental building block for the fabrication of the advanced integrated circuit.[51] Nanogap also has wide applications in areas such as rectifiers[52] and switches[53] [54], SERS detection[55], MEMS [56], and so on.[57] A wide range of technologies have been studied and used to fabricate nanogap including chemical synthesis of identical molecules electrodes, mechanical break junctions[58], shadow mask evaporation[59], top-down lithography methods such as EBL and focused ion beam (FIB) lithography[60] [61], electron-beam-induced deposition[62], and scanning probe and atomic force microscopy lithography[63] as well. Among these methods, the electron beam lithography is relatively reliable, reproducible and convenient for prototyping.

In this part, a new method of nanogap fabrication, which uses two times electron beam exposure with different acceleration energy to define patterns, will be reported. Under appropriate conditions, this method can achieve 10 nm to 15 nm gap. Gaps under 10 nm can also be achieved occasionally, but not reliably.

Generally, the resolution of fabricating nanogap is limited in part by the proximity effect.[64] Different from the beam focusing problem, which can be alleviated by applying

high-quality equipment or operating more carefully, electron scattering is an intrinsic phenomenon occurring at e-beam incidence into the material. The design of this experiment utilizes a special figure of lithography aimed to relieve the proximity effect.

5.2 Two steps exposure method for nanogap fabrication

Firstly, a high energy e-beam, practically 25 KeV, is used for defining a pair of lines with a narrow gap. Then, using the low energy of 4 KeV, two large square structures were exposed next to the lines on two sides. As shown in Figure 5.1, the combination of line and square by overlapping two lithography layers forms two large rectangles separately, which may be processed to fabricate electrodes in the following steps. The gap between the two lines written in high voltage, now, becomes the gap between the two electrodes.

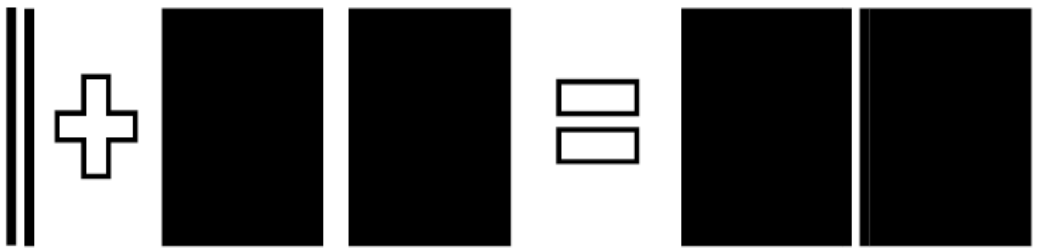

Figure 5.1: Patterns exposed on high and low voltage, where overlapping of two structures leads to the final electrode structure electrodes.

Generally, the proximity effect of EBL is more significant at low voltage[65]. The designed boundary is “blurred” because the resist on the outer edge is also exposed by the forward scattering electrons deviated from their original trace. This unexpected exposed area on which the deposited energy is enough to degrade the resist reaches to at least 30

nm ranges[66]. However, in this case, this transfer region is covered by two thin lines inside between them[67]. Since they are exposed at high voltage, the forward scattering of it is small and negligible[68]. Instead, backward scattering dominates, which is greatly "diluted" (i.e., low dose/area) because the range of backscattering is very large[69].

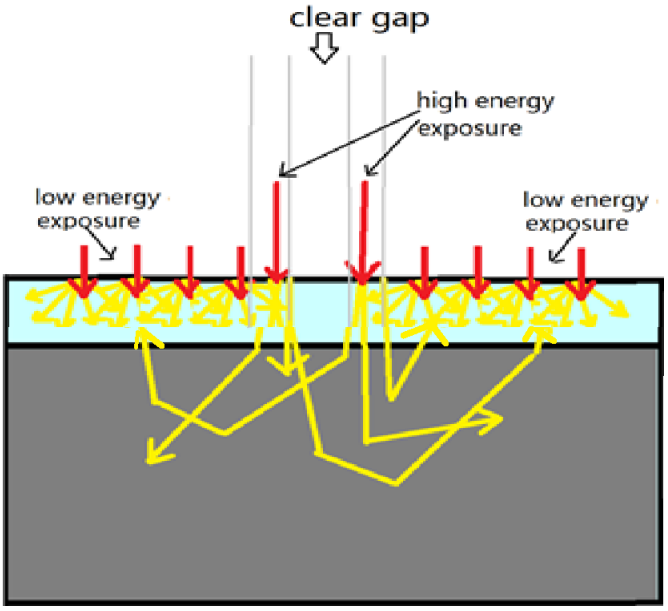

Figure 5.2 Proximity effect analysis.

Generally, in the case of proximity effect, an e-beam with energy greater than 20 KeV can be considered as high energy. Compared with the forward scattering, the backward scattering will drive electrons to move a farther distance from the position of incidence, and since its dispersion area is larger, the outer area of the designed figures will be subjected to lower dose than forward scattering (although the total leaking energy is higher than low voltage). If the leakage intensity is under the sensitivity threshold of the utilized resist[70], such scattering will not cause significant distortion of the designed pattern.

Considering that, we expected the inner sideline pairs lithographed in high voltage could achieve a high resolution.

One primary question of this idea is why a high voltage isn't applied alone for the whole square structure. Admittedly, using high energy e-beam is an effective resolution enhancement method especially for small size structure[71]. However, in this specific case, when a large size electrode is built up, if just high voltage e-beam is used, the resist on gap area would be affected by not only the nearby area but also area far from the boundary. So, the undesired dose deposited on the gap will be accumulated from a large area. In short, for a large structure, the higher voltage utilized, the lower contrast between the gap and the electrode becomes.

Someone may also ask why dose correction is not used here to deal with this problem. Dose correction based on electron trajectory simulation is one of the most common methods to deal with the proximity effect. It can calculate the possibility of an electron deviating from the designed position and moving away by what vector, and, further, by adjusting the dose of the incidence beam. It tries to achieve a pattern with the ideal feature. However, since the proximity effect is random for individual electrons, simulation is only valid on statistics of an abundance of electrons. It is unable to increase the contrast between exposed and unexposed area which is adjacent to each other. In words, it cannot increase the resolution of the edge.

5.3 Experiment

PMMA resist in anisole is selected in this experiment, and the silicon substrate is cleaned by Reactive Ion Etching (RIE) in O_2 plasma cleaning recipe for 5 mins, followed by ultrasonic cleaning in acetone then rinsed by isoprokpanol alcohol (IPA). To get a high-resolution result, a 30 nm thick film was utilized[72]. After spin coating, the sample is baked at 180℃ for 20 mins to get rid of residual solvent. Finally, the measured resist film thickness is 34 nm.

Lithography is taken on the Raith 150 system. To acquire a tightly focused beam, exposure is operated with a step size of 6 nm, the aperture size of 10 μm and a working distance of 8 mm. The corresponding beam current is 15.42 pC and 28.36 pC at 4 KeV and 25 KeV respectively[73]. After exposure, the sample is developed by MIBK: IPA 1:3.

To enhance the resolution, low-temperature development is decided to be applied finally. As the previously published paper by Bryan Cord shows, when temperature decreases from 15°C to -15°C, there is a nearly linear increase in contrast. At temperatures below -15°C though, this trend reverses[74]. Based on the real condition in our lab, the temperature increased from -14°C to -11°C during the development. All of the results of the final test and comparison test are acquired from one sample in a one-time development. Therefore, the final conclusion as a proof of concept is valid.

5.3.1 Exposure of single line pattern at high KeV

This test is to determine to the appropriate dose for the development condition and to explore the ultimate resolution, or how narrow width of the line can be achieved under the present condition. The line patterns are exposed at 25 KeV.

Single lines with a width of 4 nm, 6 nm, 10 nm, 15 nm, 20 nm, 30 nm, 40 nm and 50 nm are exposed at 25 KeV, with step size 6 nm and dose range from 270 μC/cm2 to 496.4 μC/cm2, where the dose factor is 1.07. Lines are well separated from each other with 12.5 μm, on which proximity effect between individual lines can be ignored. Development time is 1 minute for low-temperature development, and a test of 30 seconds was taken at room temperature as a comparison. Other parameters are the same as before.

The designed pattern is shown in Figure 5.3. From left to right the width increases gradually. Also from bottom to up, the dose is increased.

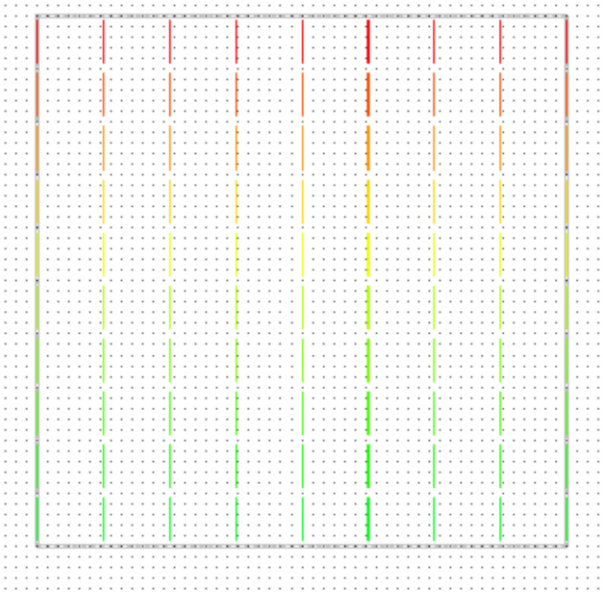

Figure 5.3 Pattern design of lines

5.3.2 Exposure of gap between two narrow lines at high KeV

This test is to explore how narrow gap can be achieved between two lines. Since the line pairs, exposed at a high voltage, are applied to cover the blur edges of the large pattern exposed by low voltage beam, the wider line pairs can enlarge the gap between the two low-voltage pads, and furtherly decrease the proximity effect. Therefore, the line width is expected to be the wider, the better. However, as it is discussed before, if the line is designed too wide, the backward scattering of the electrons will aggravate and decrease the resolution reversely. In this experiment, different width of lines are also tested to see how wide the line is tolerable.

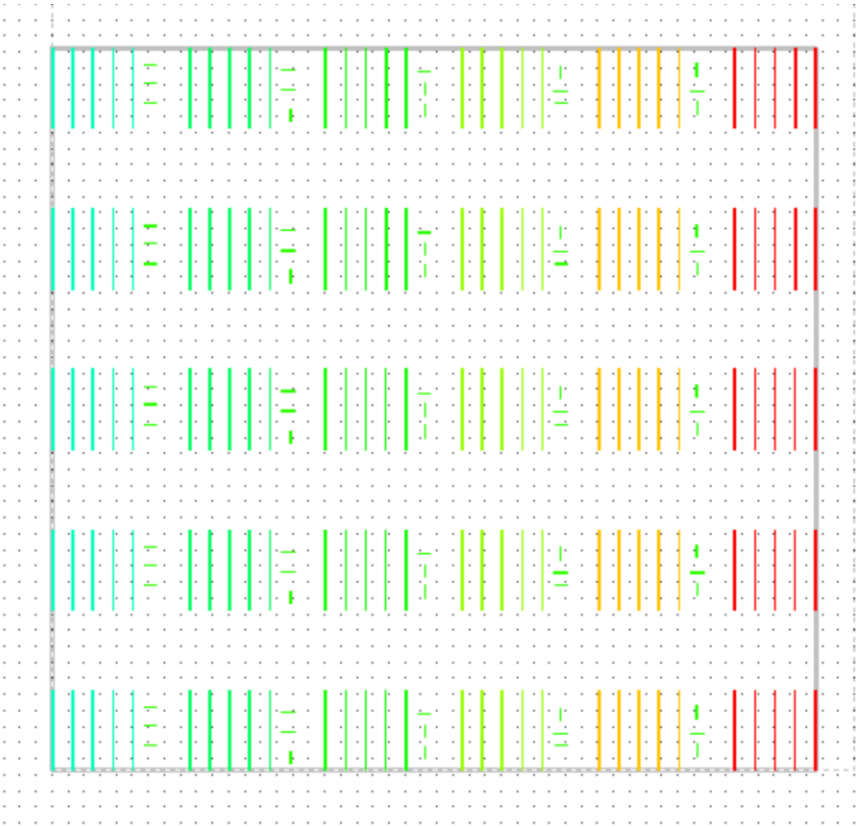

Figure 5.4 Pattern design of the gap test

The design pattern is shown in Figure 5.4. On each line array, the gaps are increasing from 10 nm to 30 nm, in 5 nm steps. From bottom to up, the width of line pairs is decreasing from 70 nm to 30 nm. And the dose is increased from 300 μC/cm2 to 497.7 μC/cm2, with a dose factor of 1.2. Since the two lines in one pair are close enough to affect each other, the necessary dose is expected to be lower than a single line.

5.3.3 Exposure of gap between two large pads at low (for large square) and high (for line pair) KeV

On the final experiment, our idea is to overlap two layers of lithography. One layer involves line array exposed in 25 KeV, and the other layer involves large square array exposed in 4 KeV. Dose and other parameters are determined in the above sections.

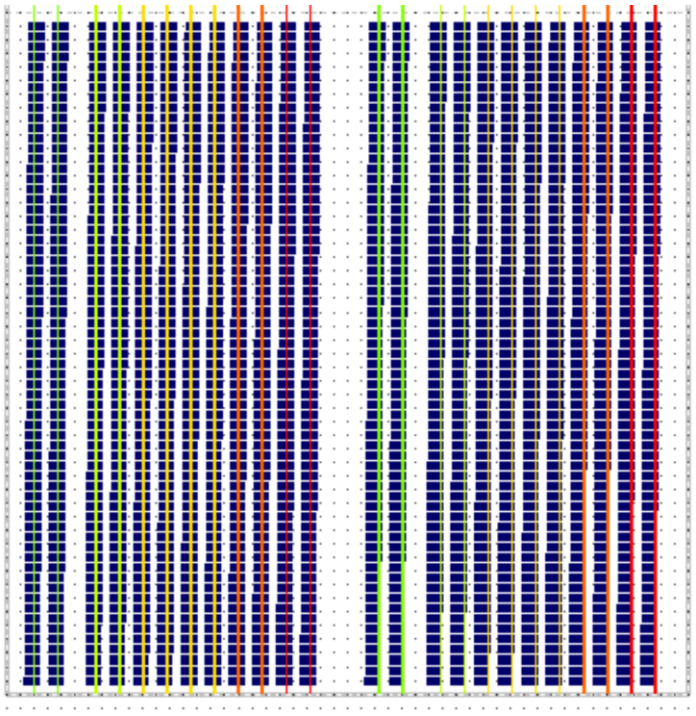

Figure 5.5 Final pattern design

The most challenging part is the alignment of the two layers. Therefore, we designed an array of squares with relative position shift to the layer of lines. The position shift between two square pairs next to each other is 10 nm. The total tolerance of each writing field is 2.5μm on my sample.

To verify the idea of this experiment that it can effectively alleviate the result of proximity effect, a comparison experiment is also carried out, which expose large square pairs at low or high voltage individually. All the parameters including the resist thickness, development time and so on are kept as same as the major experiment.

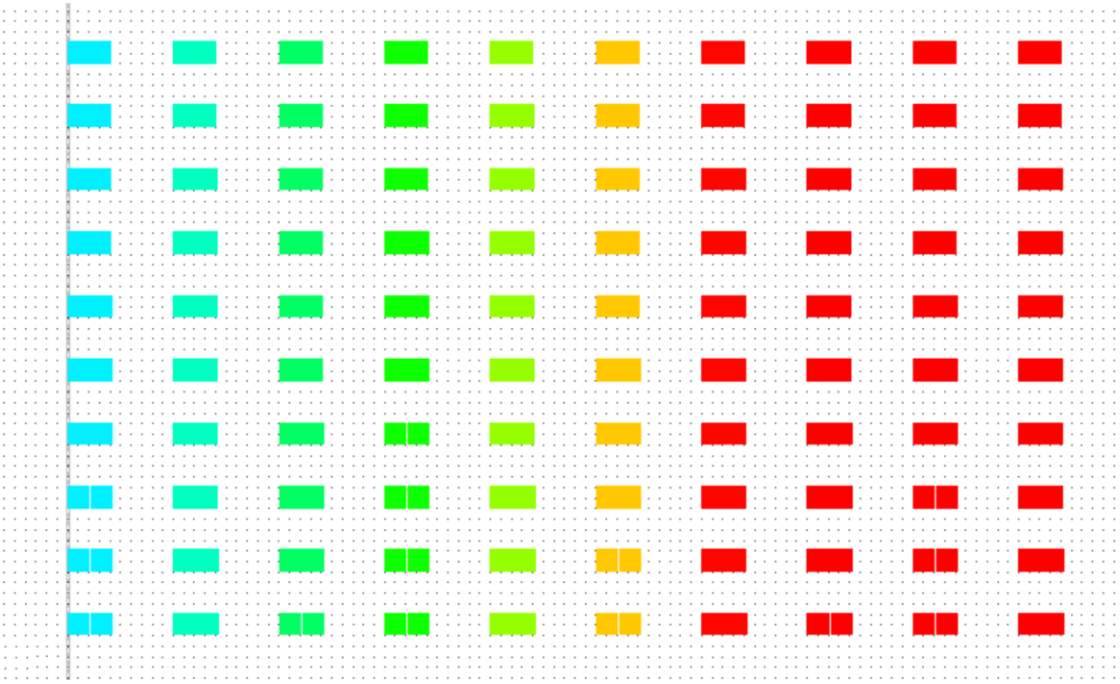

Figure 5.6 Design pattern of comparison test

The design pattern is shown in Figure 5.6. The gap size between two squares varies from 10 nm to 100 nm, with the step of 10 nm. From left to right dose increases with dose

factor of 1.2. For 4 KeV, the dose changes from 50 μC/cm^2 to 258 μC/cm^2, and for 25 KeV, the dose changes from 100 μC/cm^2 to 516 μC/cm^2.

5.4 Result and analysis

5.4.1 Line pattern result

The result of line pattern test shows that the appropriate dose of exposure in this experiment is about 350 μC/cm^2, and the best result is about 16 nm wide.

5.4.2 Gap between two lines

Figure 5.7 shows one of the line pair arrays as an example, for which the designed gap size is 20 nm fixed. The difference from left to right is the width of line decreasing from 70 nm to 30 nm. The exposure dose is 345.6 μC/cm^2. Due to the proximity effect, the wider line pattern will give more dose of exposure to its neighboring area. This trend is in agreement with our expectation.

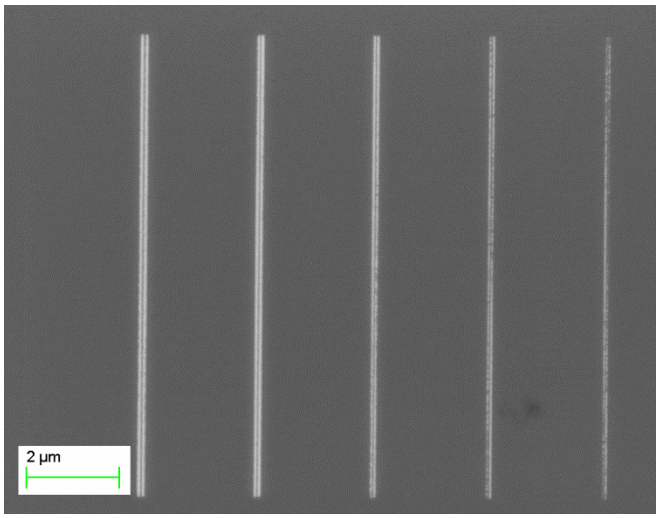

Figure 5.7 Image result of line pairs array. From left to right the dose looks like decreasing, but, in fact, the dose is constant

As we have seen before, the appropriate doses for different width and gap combination are different. I measured all the line pairs with a fixed dose, and all of them can achieve gap size under 15 nm. Some of them can achieve a narrow gap under 10 nm.

As expected, wider line or pattern with higher dose tends to expand to two sides. And therefore, the gap will be narrowed from its original size as designed. In this case, the patterns with a large designed gap, such as 20 nm or 30 nm, are also possible to produce a small gap with several tens nm or under 10 nm. Figure 5.8 is a comparison of the wide line pattern, figure a), and narrow line pattern, figure b).

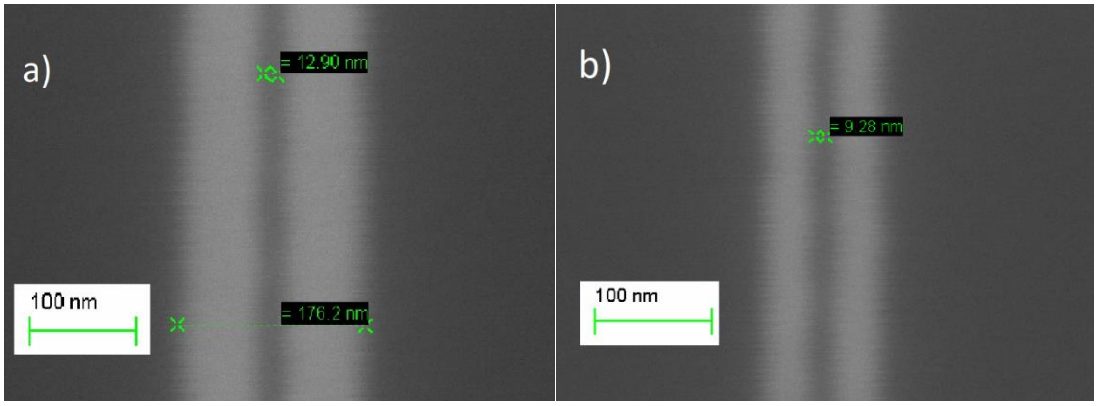

Figure 5.8 a) Image result of line pairs with the narrow gap a) dose is 497.7 uC/cm², width is 70 nm, and the designed gap is 25 nm; b) dose is 345.6 uC/cm². Designed width is 40 nm width and gap is 15 nm

Since these line pairs exposed in high energy are used to cover the edge of the large pattern exposed at low voltage, the wider line pairs are desired. However, if we compare these two pictures carefully, we can find that in figure a), the color of the gap area is lighter and relatively close to the exposed area, which implies that the residue resist covering gap area is thinner than what we get by using narrow line pattern. This is not good for the

following processes, such as RIE. Obviously, due to the proximity effect, the gap area will be exposed more in the case with a wider line.

Given the result of the gap test, it is found that the highest tolerable width of the line in this case is about 40 nm.

5.4.3 Exposure of big squares at low keV as a comparison

Figure 5.9 shows the result of square pairs with a narrow gap that is exposed at 4 keV. As expected theoretically, the proximity effect is serious, and the resolution is very low.

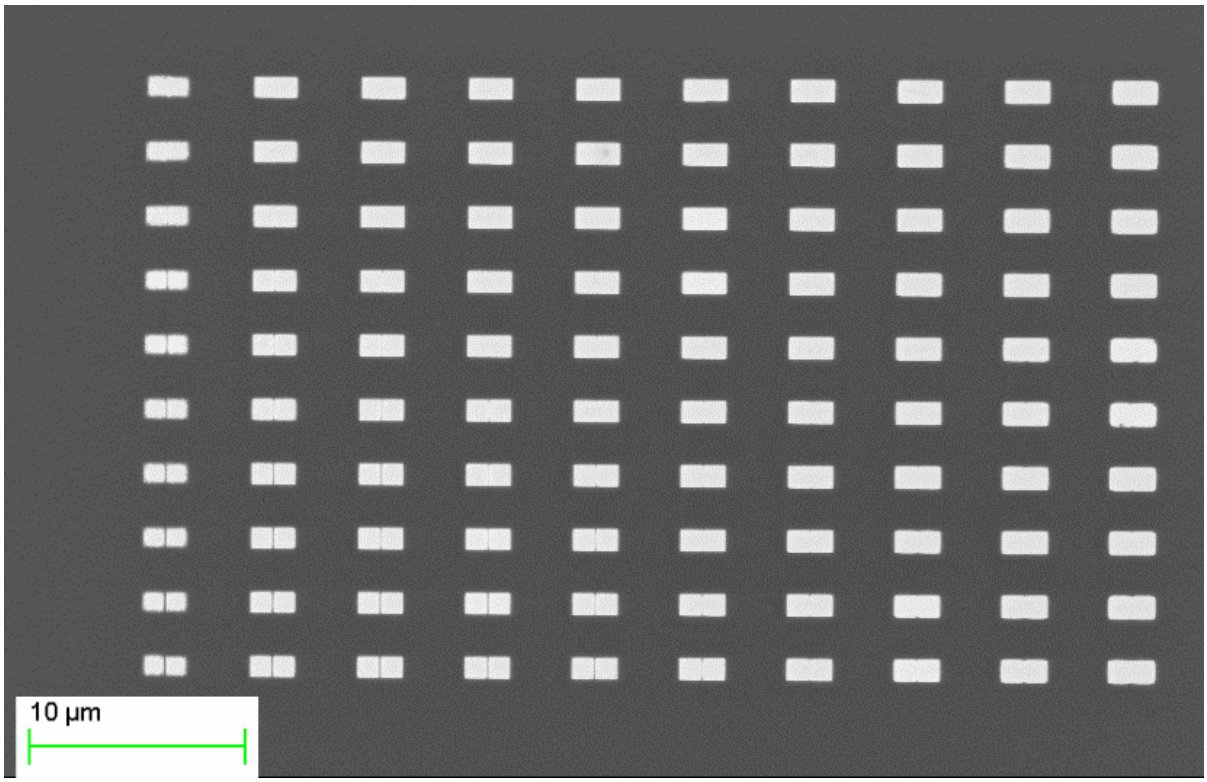

Figure 5.9 Large pattern test using 25 KeV alone

We zoomed-in one of the square pairs which is in the third column and fourth row, for which the dose is 72 µC/cm^2, and the designed gap size is 40 nm. The result is shown

in figure 5.10. The measured gap size is 19.45 nm in the area nearby up and bottom sides. However, the two patterns merged together in the middle.

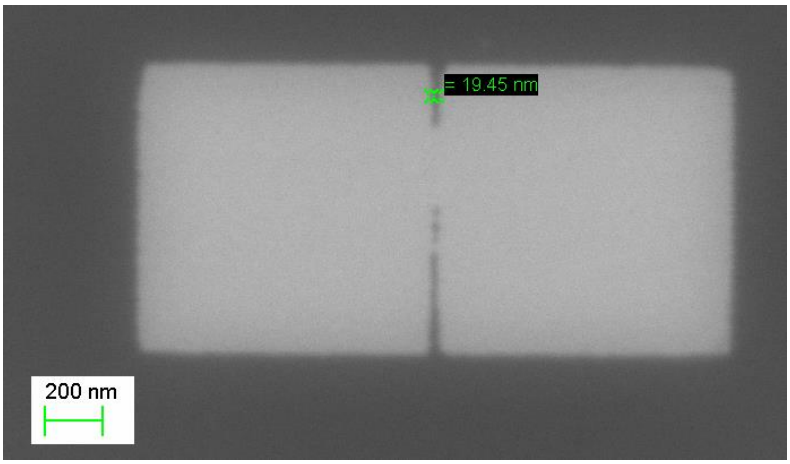

Figure 5.10 Zoom in image of the square pairs with the best result using 4 KeV alone

The figure 5.11 shows the result of exposure using 25 KeV alone, where the proximity effect is not as serious as using 4 KeV. The best result appears at the pair with a dose of 358.3 μC/cm2 and a designed gap of 20 nm, see figure 5.12. The measured gap is 18 nm. However, the contrast between the gap area and the square pattern is very low, which implies little resist remains.

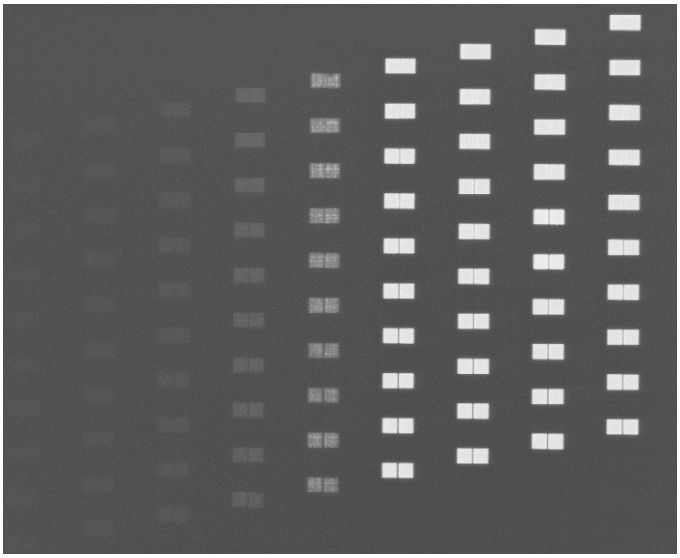

Figure 5.11 Large pattern test using 25 KeV alone

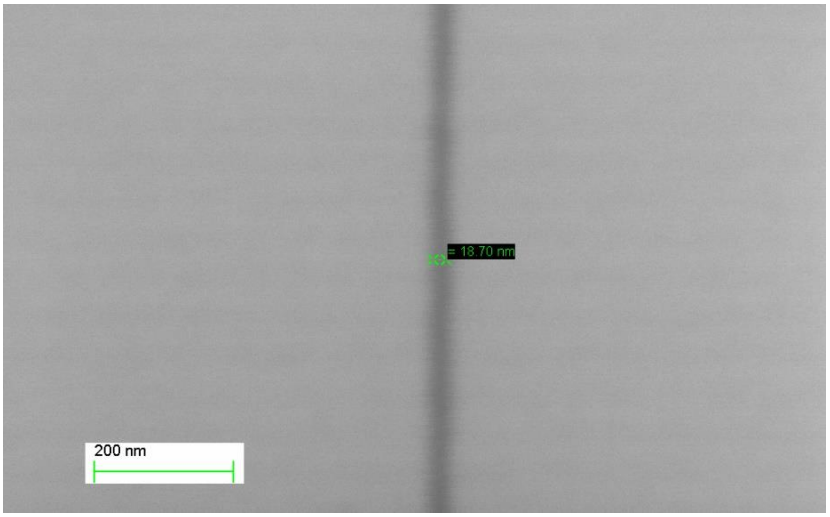

Figure 5.12 Zoom in image of the gap area of the best result using 25 KeV alone

5.4.4 Final results

Figure 5.12 is the imaging result of the final test using the combination of exposure of 4 KeV and 25 KeV. The measured gap is 12.40 nm, and the edges between the gap and the exposed patterns are very clear.

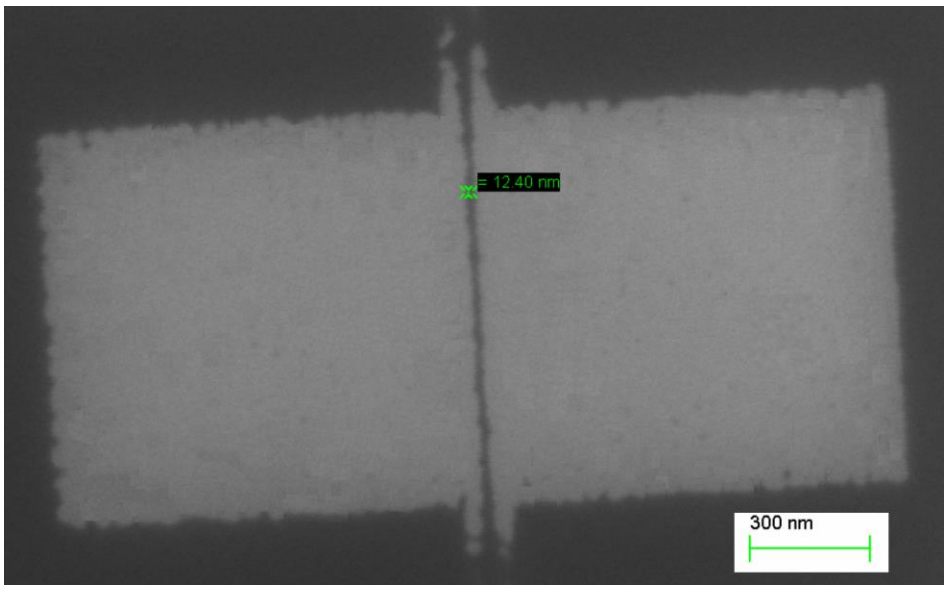

Figure 5.12 Result of using two times exposure at high and low voltage change the font for figure caption, to make it consistent throughout the thesis

Reference

[1] Present, I. J. R. i. c. a. (2000). "Cramming more components onto integrated circuits." Readings in computer architecture, 56.

[2] Allan, A., Edenfeld, D., Joyner, W.H., Kahng, A.B., Rodgers, M. and Zorian, Y., 2002. 2001 technology roadmap for semiconductors. *Computer*, *35*(1), pp.42-53.

[3] Drexler, E., 1986. Engines of Creation: The Coming Era of Nanotechnology and Nanosystems: Molecular Machinery, Manufacturing, and Computation.

[4] Smith, D.L., 1995. *Thin-film deposition: principles and practice*(Vol. 108). New York etc: McGraw-hill.

[5] Dolan, G.J., 1977. Offset masks for lift-off photoprocessing. *Applied Physics Letters*, *31*(5), pp.337-339.

[6] Groechel, D.W., Taylor, B., Henri, J.R. and Obinata, N., Applied Materials Inc, 1991. *Process for RIE etching silicon dioxide*. U.S. Patent 5,021,121.

[7] Hector, S., 1998. Status and future of X-ray lithography. *Microelectronic engineering*, *41*, pp.25-30.

[8] Tormen, M., Businaro, L., Altissimo, M., Romanato, F., Cabrini, S., Perennes, F., Proietti, R., Sun, H.B., Kawata, S. and Di Fabrizio, E., 2004. 3D patterning by means of nanoimprinting, X-ray and two-photon lithography. *Microelectronic Engineering*, *73*, pp.535-541.

[9] Levenson, M.D., Viswanathan, N.S. and Simpson, R.A., 1982. Improving resolution in photolithography with a phase-shifting mask. *IEEE Transactions on electron devices*, *29*(12), pp.1828-1836

[10] Vogel, H., Simon, K. and Derksen, A.T.A.M., ASML Holding NV, 2005. *Immersion photolithography system and method using microchannel nozzles*. U.S. Patent 6,867,844.

[11] Davies, G., Stoeldraijer, J., Heskamp, B., Mulkens, J., Sytsma, J., Bakker, H., Glatzel, H., Wagner, C., Roempp, O. and Boerret, R., 1998. 193 nm step and scan lithography. In *SEMI Technology Symposium* (Vol. 98, pp. 1-15)

[12] Nalamasu, O., Cheng, M., Timko, A.G., Pol, V., Reichmanis, E. and Thompson, L.F., 1991. An overview of resist processing for deep-UV lithography. *Journal of Photopolymer Science and Technology*, *4*(3), pp.299-318.

[13] Hudyma, R.M., 2002, December. An overview of optical systems for 30 nm resolution lithography at EUV wavelengths. In *International Optical Design Conference 2002* (Vol. 4832, pp. 137-149). International Society for Optics and Photonics

[14] *Merritt, Rick (8 Feb 2017), "TSMC, Samsung Diverge at 7nm", www.eetimes.com*

[15] Pain, L., Icard, B., Manakli, S., Todeschini, J., Minghetti, B., Wang, V. and Henry, D., 2006. Transitioning of direct e-beam write technology from research and development into production flow. *Microelectronic Engineering*, *83*(4-9), pp.749-753.

[16] Pease, R.F.W., 1981. Electron beam lithography. *Contemporary Physics*, *22*(3), pp.265-290.

[17] Vieu, C., Carcenac, F., Pepin, A., Chen, Y., Mejias, M., Lebib, A., Manin-Ferlazzo, L., Couraud, L. and Launois, H., 2000. Electron beam lithography: resolution limits and applications. *Applied surface science*, *164*(1-4), pp.111-117.

[18] Wu, C.S., Makiuchi, Y. and Chen, C., 2010. High-energy electron beam lithography for nanoscale fabrication. In *Lithography*. InTech.

[19] Shelton, H., 1957. Thermionic emission from a planar tantalum crystal. *Physical Review*, *107*(6), p.1553.

[20] Swanson, L.W. and Schwind, G.A., 2008. Review of ZrO/W schottky cathode. In *Handbook of Charged Particle Optics, Second Edition* (pp. 1-28). CRC Press.

[21] Mohammad, M.A., Muhammad, M., Dew, S.K. and Stepanova, M., 2012. Fundamentals of electron beam exposure and development. In *Nanofabrication* (pp. 11-41). Springer, Vienna.

[22] Moodera, J.S., Kinder, L.R., Wong, T.M. and Meservey, R., 1995. Large magnetoresistance at room temperature in ferromagnetic thin film tunnel junctions. *Physical review letters*, *74*(16), p.3273.

[23] Lin, L.H. and Beauchamp, H.L., 1973. High speed beam deflection and blanking for electron lithography. *Journal of Vacuum Science and Technology*, *10*(6), pp.987-990.

[24] Terris, B.D. and Thomson, T., 2005. Nanofabricated and self-assembled magnetic structures as data storage media. *Journal of physics D: Applied physics*, *38*(12), p.R199.

[25] Duan, H., Winston, D., Yang, J.K., Cord, B.M., Manfrinato, V.R. and Berggren, K.K., 2010. Sub-10-nm half-pitch electron-beam lithography by using poly (methyl

methacrylate) as a negative resist. *Journal of Vacuum Science & Technology B, Nanotechnology and Microelectronics: Materials, Processing, Measurement, and Phenomena*, *28*(6), pp.C6C58-C6C62.

[26] Li, T., Hu, W. and Zhu, D., 2010. Nanogap electrodes. *Advanced Materials*, *22*(2), pp.286-300.

[27] Manfrinato, V.R., Zhang, L., Su, D., Duan, H., Hobbs, R.G., Stach, E.A. and Berggren, K.K., 2013. Resolution limits of electron-beam lithography toward the atomic scale. *Nano letters*, *13*(4), pp.1555-1558.

[28] Lorenz, H., Despont, M., Fahrni, N., LaBianca, N., Renaud, P. and Vettiger, P., 1997. SU-8: a low-cost negative resist for MEMS. *Journal of Micromechanics and Microengineering*, *7*(3), p.121.

[29] Fujita, J., Ohnishi, Y., Ochiai, Y., Nomura, E. and Matsui, S., 1996. Nanometer-scale resolution of calixarene negative resist in electron beam lithography. *Journal of Vacuum Science & Technology B: Microelectronics and Nanometer Structures Processing, Measurement, and Phenomena*, *14*(6), pp.4272-4276.

[30] Ma, S., Con, C., Yavuz, M. and Cui, B., 2011. Polystyrene negative resist for high-resolution electron beam lithography. *Nanoscale research letters*, *6*(1), p.446.

[31] Yang, J.K., Anant, V. and Berggren, K.K., 2006. Enhancing etch resistance of hydrogen silsesquioxane via postdevelop electron curing. *Journal of Vacuum Science & Technology B: Microelectronics and Nanometer Structures Processing, Measurement, and Phenomena*, *24*(6), pp.3157-3161.

[32] Namatsu, H., Yamaguchi, T., Nagase, M., Yamazaki, K. and Kurihara, K., 1998. Nano-patterning of a hydrogen silsesquioxane resist with reduced linewidth fluctuations. *Microelectronic Engineering*, *41*, pp.331-334.

[33] Grigorescu, A.E., Van der Krogt, M.C., Hagen, C.W. and Kruit, P., 2007. 10 nm lines and spaces written in HSQ, using electron beam lithography. *Microelectronic Engineering*, *84*(5-8), pp.822-824.

[34] Yang, J.K., Cord, B., Duan, H., Berggren, K.K., Klingfus, J., Nam, S.W., Kim, K.B. and Rooks, M.J., 2009. Understanding of hydrogen silsesquioxane electron resist for sub-5-nm-half-pitch lithography. *Journal of Vacuum Science & Technology B: Microelectronics and Nanometer Structures Processing, Measurement, and Phenomena*, *27*(6), pp.2622-2627.

[35] Product Sheet H-SiOx. https://www.aqmaterials.com/aqm-silsesquioxane-polymers

[36] Clark, N., Vanderslice, A., Grove III, R. and Krchnavek, R.R., 2006. Time-dependent exposure dose of hydrogen silsesquioxane when used as a negative electron-beam resist. *Journal of Vacuum Science & Technology B: Microelectronics and Nanometer Structures Processing, Measurement, and Phenomena*, *24*(6), pp.3073-3076.

[37] Cord, B.M., 2009. *Achieving sub-10-nm resolution using scanning electron beam lithography* (Doctoral dissertation, Massachusetts Institute of Technology).

[38] Henschel, W., Georgiev, Y.M. and Kurz, H., 2003. Study of a high contrast process for hydrogen silsesquioxane as a negative tone electron beam resist. *Journal of Vacuum Science & Technology B: Microelectronics and Nanometer Structures Processing,*

Measurement, and Phenomena, *21*(5), pp.2018-2025..

[39] Chen, Y., Yang, H. and Cui, Z., 2006. Effects of developing conditions on the contrast and sensitivity of hydrogen silsesquioxane. *Microelectronic Engineering*, *83*(4-9), pp.1119-1123.

[40] Sidorkin, V., van der Drift, E. and Salemink, H., 2008. Influence of hydrogen silsesquioxane resist exposure temperature on ultrahigh resolution electron beam lithography. *Journal of Vacuum Science & Technology B: Microelectronics and Nanometer Structures Processing, Measurement, and Phenomena*, *26*(6), pp.2049-2053.

[41] Grigorescu, A.E., Van der Krogt, M.C., Hagen, C.W. and Kruit, P., 2007. 10 nm lines and spaces written in HSQ, using electron beam lithography. *Microelectronic Engineering*, *84*(5-8), pp.822-824.

[42] Nam, S.W., Rooks, M.J., Yang, J.K., Berggren, K.K., Kim, H.M., Lee, M.H., Kim, K.B., Sim, J.H. and Yoon, D.Y., 2009. Contrast enhancement behavior of hydrogen silsesquioxane in a salty developer. *Journal of Vacuum Science & Technology B: Microelectronics and Nanometer Structures Processing, Measurement, and Phenomena*, *27*(6), pp.2635-2639.

[43] Yang, J.K. and Berggren, K.K., 2007. Using high-contrast salty development of hydrogen silsesquioxane for sub-10-nm half-pitch lithography. *Journal of Vacuum Science & Technology B: Microelectronics and Nanometer Structures Processing, Measurement, and Phenomena*, *25*(6), pp.2025-2029.

[44] Yang, J.K. and Berggren, K.K., 2007. Using high-contrast salty development of hydrogen silsesquioxane for sub-10-nm half-pitch lithography. *Journal of Vacuum Science & Technology B: Microelectronics and Nanometer Structures Processing, Measurement, and Phenomena*, *25*(6), pp.2025-2029

[45] Jeyakumar, A. and Henderson, C.L., 2004, May. Enhancing the electron beam sensitivity of hydrogen silsesquioxane (HSQ). In *Advances in Resist Technology and Processing XXI*(Vol. 5376, pp. 490-502). International Society for Optics and Photonics.

[46] Newman, T.H., Pease, R.F.W. and DeVore, W., 1983. Dot matrix electron beam lithography. *Journal of Vacuum Science & Technology B: Microelectronics Processing and Phenomena*, *1*(4), pp.999-1002.

[47] Li, L., Fang Lim, S., Puretzky, A.A., Riehn, R. and Hallen, H.D., 2012. Near-field enhanced ultraviolet resonance Raman spectroscopy using aluminum bow-tie nano-antenna. *Applied physics letters*, *101*(11), p.113116.

[48] Cord, B., Yang, J., Duan, H., Joy, D.C., Klingfus, J. and Berggren, K.K., 2009. Limiting factors in sub-10 nm scanning-electron-beam lithography. *Journal of Vacuum Science & Technology B: Microelectronics and Nanometer Structures Processing, Measurement, and Phenomena*, *27*(6), pp.2616-2621.

[49] Pease, R.F.W., 1981. Electron beam lithography. *Contemporary Physics*, *22*(3), pp.265-290.

[50] Van Delft, F.C., 2002. Delay-time and aging effects on contrast and sensitivity of hydrogen silsesquioxane. *Journal of Vacuum Science & Technology B: Microelectronics*

and Nanometer Structures Processing, Measurement, and Phenomena, *20*(6), pp.2932-2936.

[51] Kang, S.M. and Leblebici, Y., 2003. *CMOS digital integrated circuits*. Tata McGraw-Hill Education.

[52] Metzger, R.M., Chen, B., Höpfner, U., Lakshmikantham, M.V., Vuillaume, D., Kawai, T., Wu, X., Tachibana, H., Hughes, T.V., Sakurai, H. and Baldwin, J.W., 1997. Unimolecular electrical rectification in hexadecylquinolinium tricyanoquinodimethanide. *Journal of the American Chemical Society*, *119*(43), pp.10455-10466.

[53] Collier, C.P., Mattersteig, G., Wong, E.W., Luo, Y., Beverly, K., Sampaio, J., Raymo, F.M., Stoddart, J.F. and Heath, J.R., 2000. A [2] catenane-based solid state electronically reconfigurable switch. *Science*, *289*(5482), pp.1172-1175.

[54] Blum, A.S., Kushmerick, J.G., Long, D.P., Patterson, C.H., Yang, J.C., Henderson, J.C., Yao, Y., Tour, J.M., Shashidhar, R. and Ratna, B.R., 2005. Molecularly inherent voltage-controlled conductance switching. *Nature Materials*, *4*(2), p.167.

[55] Su, M. and Liu, H., 2018. Plasmonic Nanomaterials for SERS Detection of Environmental Pollutants. *Nanotechnology in Environmental Science*, pp.473-514.

[56] Lee, B.H., Moon, D.I., Jang, H., Kim, C.H., Seol, M.L., Choi, J.M., Lee, D.I., Kim, M.W., Yoon, J.B. and Choi, Y.K., 2014. A mechanical and electrical transistor structure (METS) with a sub-2 nm nanogap for effective voltage scaling. *Nanoscale*, *6*(14), pp.7799-7804.

[57] Li, T., Hu, W. and Zhu, D., 2010. Nanogap electrodes. *Advanced Materials*, *22*(2), pp.286-300.

[58] Reed, M.A., Zhou, C., Muller, C.J., Burgin, T.P. and Tour, J.M., 1997. Conductance of a molecular junction. *Science*, *278*(5336), pp.252-254.

[59] Kubatkin, S., Danilov, A., Hjort, M., Cornil, J., Brédas, J.L., Stuhr-Hansen, N., Hedegård, P. and Bjørnholm, T., 2003. Single-electron transistor of a single organic molecule with access to several redox states. *Nature*, *425*(6959), p.698.

[60] Nagase, T., Kubota, T. and Mashiko, S., 2003. Fabrication of nano-gap electrodes for measuring electrical properties of organic molecules using a focused ion beam. *Thin Solid Films*, *438*, pp.374-377.

[61] Nagase, T., Gamo, K., Kubota, T. and Mashiko, S., 2006. Direct fabrication of nano-gap electrodes by focused ion beam etching. *Thin Solid Films*, *499*(1-2), pp.279-284.

[62] Bezryadin, A. and Dekker, C., 1997. Nanofabrication of electrodes with sub-5 nm spacing for transport experiments on single molecules and metal clusters. *Journal of Vacuum Science & Technology B: Microelectronics and Nanometer Structures Processing, Measurement, and Phenomena*, *15*(4), pp.793-799.

[63] Notargiacomo, A., Foglietti, V., Cianci, E., Capellini, G., Adami, M., Faraci, P., Evangelisti, F. and Nicolini, C., 1999. Atomic force microscopy lithography as a nanodevice development technique. *Nanotechnology*, *10*(4), p.458.

[64] Ren, L. and Chen, B., 2004, October. Proximity effect in electron beam lithography. In *Solid-State and Integrated Circuits Technology, 2004. Proceedings. 7th International Conference on* (Vol. 1, pp. 579-582). IEEE.

[65] Pease, R.F.W., 1981. Electron beam lithography. *Contemporary Physics*, *22*(3), pp.265-290.

[66] Bolorizadeh, M. and Joy, D.C., 2007. Effects of fast secondary electrons to low-voltage electron beam lithography. *Journal of Micro/Nanolithography, MEMS, and MOEMS*, *6*(2), p.023004.

[67] Han, G., Khan, M., Fang, Y. and Cerrina, F., 2002. Comprehensive model of electron energy deposition. *Journal of Vacuum Science & Technology B: Microelectronics and Nanometer Structures Processing, Measurement, and Phenomena*, *20*(6), pp.2666-2671.

[68] Anderson, E.H., Olynick, D.L., Chao, W., Harteneck, B. and Veklerov, E., 2001. Influence of sub-100 nm scattering on high-energy electron beam lithography. *Journal of Vacuum Science & Technology B: Microelectronics and Nanometer Structures Processing, Measurement, and Phenomena*, *19*(6), pp.2504-2507.

[69] Hawryluk, R.J., Hawryluk, A.M. and Smith, H.I., 1974. Energy dissipation in a thin polymer film by electron beam scattering. *Journal of Applied Physics*, *45*(6), pp.2551-2566.

[70] Greeneich, J.S., 1974. Solubility Rate of Poly-(Methyl Methacrylate), PMMA, Electron-Resist. *Journal of The Electrochemical Society*, *121*(12), pp.1669-1671.

[71] Hudek, P. and Beyer, D., 2006. Exposure optimization in high-resolution e-beam lithography. *Microelectronic Engineering*, *83*(4-9), pp.780-783.

[72] Greeneich, J.S. and Van Duzer, T., 1974. An exposure model for electron-sensitive resists. *IEEE Transactions on Electron Devices*, *21*(5), pp.286-299.

[73] Anderson, E.H., Olynick, D.L., Chao, W., Harteneck, B. and Veklerov, E., 2001. Influence of sub-100 nm scattering on high-energy electron beam lithography. *Journal of Vacuum Science & Technology B: Microelectronics and Nanometer Structures Processing, Measurement, and Phenomena*, *19*(6), pp.2504-2507.

[74] Hu, W., Sarveswaran, K., Lieberman, M. and Bernstein, G.H., 2004. Sub-10 nm electron beam lithography using cold development of poly (methylmethacrylate). *Journal of Vacuum Science & Technology B: Microelectronics and Nanometer Structures Processing, Measurement, and Phenomena*, *22*(4), pp.1711-1716.